LOAD AND STRESS ANALYSIS OF CYLINDRICAL WORM GEARING USING TOOTH SLICING METHOD

A.H. Falah and A.H. Elkholy
Mechanical Engineering Department
Kuwait University
KUWAIT
Email: afalah@kuc01.kuniv.edu.kw

Received March 2005, Accepted October 2005
No. 05-CSME-10, E.I.C. Accession 2862

ABSTRACT

A method for the determination of load and stress distributions of the instantaneously engaged teeth of cylindrical worm gears is represented in this paper. The method is based on the assumption that both the worm and gear can be modeled as a series of spur gear slices. The exact geometry and point of load application of each slice depends on its location within the mesh. By calculating the applied load and stress for each slice, the same can be determined for the entire worm gear set. The method takes into consideration tooth stiffness variation from root to tip, tooth bending deflection, local contact deformation, tooth foundation deformation and, the influence of gear parameters on load and stress. Calculated results were found to be in agreement with experimental and analytical ones obtained from literature under given operating conditions.

Keywords: Gear, Load/Stress Distribution, Worm, Wheel, Tooth Stiffness, Contact Line, Line of Action.

ANALYSE DES CHARGES ET DES CONTRAINTES DES ENGRENAGES CYLINDRIQUES À VIS À L'AIDE DE LA MÉTHODE DE DÉCOUPAGE EN TRANCHES

RESUME

Une méthode de détermination de la distribution des charges et des contraintes pendant l'engrènement instantané des dents des engrenages cylindriques à vis est présentée dans cet article. La méthode est basée sur la supposition que la vis sans fin et la roue menée peuvent être modelées par des séries de tranches d'engrenage à denture droite. La géométrie exacte et le point d'application de la charge pour chaque tranche dépendent de son emplacement dans l'engrènement. En calculant la charge appliquée et la contrainte pour chaque tranche, les mêmes quantités peuvent être déterminées pour l'ensemble entière d'engrenage à vis. La méthode tient compte de la variation de rigidité de la dent à partir de la racine jusqu'au bout, fléchissement de dent, déformation locale au contact, déformation de la base de dent, et l'influence des paramètres de l'engrenage sur la charge et la contrainte. Les résultats de calcul ont été trouvés d'accord avec les résultats publiés, obtenus expérimentalement et analytiquement, pour des conditions d'opération données.

Mots clés: Engrenage, Distribution de Charge/Contrainte, Vis sans fin, Roue Dentée, Rigidité de Dent, Ligne de Contact, Ligne d'action.

INTRODUCTION

The load distribution along contact lines of cylindrical worm gears is considered one of the important factors affecting the performance of the gear set. The recognition of this fact is the reason for the many attempts which have been made to develop rational methods for the evaluation of load distribution. One of the main tasks in the determination of load distribution is to find a reliable method for the calculation of tooth stresses, lubrication characteristics, and scoring resistance of a given gear set. In [1-6] different methods were used for the calculation of tooth loading, stresses and deformation. An empirical formula for bending deflection was used in [1] to obtain a transformation matrix for calculating load. By combining a discretized gear model with finite element analysis (FEA), the authors in [2] were able to calculate tooth loading taking into account the varying meshing stiffness, geometric modification and elastic deflection of the engaged gears. Direct measurement of tooth loads using strain gauging under dynamic operating conditions was introduced in [3]. Another testing procedure that was devised based upon the assumption that all contact normals of tooth surface should be at right angles to the direction of displacement, was given in [4]. The authors in [5] presented a sophisticated numerical analysis and a three-dimensional simulation within an advanced CAE package to determine tooth loading. A 3D FEA model for calculating load sharing, tooth meshing stiffness and transmission errors which account for modified tooth geometry was developed in [6]. Similar FEA model combined with either regression analysis and interpolation functions [7], or solid modeling and mesh algorithm [8] were also quoted. Another technique based on contact mechanics was given in [9].

This paper introduces a new approach which is more efficient and less computer intensive than those based on a full 3D FEA model and more accurate than the traditional methods. It takes into account the varying mesh stiffness and teeth elastic deformations due to bending, shear, compression and foundation. It is based on the assumption that both the worm and gear can be discretized into a number of thin slices. Therefore, the 3D mechanical properties can be efficiently approximated using accurate 2D analyzing tools. The fundamental geometry of the gear set can then be represented by its transverse section, and a 2D model that ensures the computational precision.

2. GEAR SET GEOMETRY

The cylindrical (single enveloping) worm and gear of a set have the same hand of helix. The lead angle λ on the worm equals the helix angle ψ on the gear and the worm axial pitch p_x and the gear transverse circular pitch p_t are equal as well for a 90° shaft angle. The worm lead angle is the complement of the worm helix angle. The pitch radius of the gear R_2 is the radius measured on a plane containing the worm axis and is determined from:

$$R_2 = \frac{N_2 \; p_t}{2\pi} \tag{1}$$

where N_2 is the number of teeth on the gear. The Lead of worm L is calculated from:

$$L = \frac{p_t \cos\phi \; N_1}{\cos\lambda}$$

where ϕ is the pitch pressure angle. The center distance of the gear set C is related to the root R_r, pitch R and outside R_o radii of the worm and gear as follows:

$$\begin{aligned} C &= R_1 + R_2 \\ &= R_{r_1} + R_{o_2} \\ &= R_{o_1} + R_{r_2} \end{aligned} \tag{2}$$

where 1, 2 refer to the worm and gear, respectively. Note that the tooth clearance is neglected in equation (2).

The worm base radius is calculated from:

$$\begin{aligned} R_{b_1} &= \frac{L}{2\pi \tan\lambda} \\ &= \frac{N_1 R_2 \cos\phi}{N_2 \sin\lambda} \end{aligned} \tag{3}$$

whereas the worm form radius R_f (radius to top of fillet on worm thread) is determined from [10].

$$\begin{aligned} R_{f_1} = \text{SQRT}\{&(R_{r_1} + R_{o_2})^2 + R_{o_2}^2 \\ &- 2[R_{o_2}(R_{r_1} + R_{o_2})]\cos\beta\} \end{aligned} \tag{4}$$

where β is determined from:

$$\beta = \sin^{-1}\left[\frac{R_{b_1}}{R_{r_1} + R_{o_2}}\right] \tag{5}$$

The actual contact ratio CR of the gear set is calculated from:

$$\begin{aligned} CR = \alpha \Big[&\sqrt{R_{o_2}^2 - R_{b_2}^2} \\ &- R_2 \cos\phi \tan\lambda \\ &+ \frac{\sqrt{R_{o_1}^2 - R_{b_1}^2} - R_1}{\sin\lambda}\Big] \end{aligned} \tag{6}$$

where R_{b_2} is the base radius of the gear and is determined from

$$R_{b_2} = R_2 \cos\phi \tag{7}$$

$$\text{and} \quad \alpha = \frac{1}{L \cos\lambda}$$

The contact ratio, given in (6), is the number of teeth on the worm and gear that are in simultaneous mesh at a given instant.

3. GEAR MESH MODELING:

To facilitate the analysis and use the experience already established in literature, both the worm and gear were modeled as thin spur gear segments (slices) by a series of radial slicing planes. This approach was first introduced by Tredgold [11] for modeling helical and bevel gears. Figure (1) shows the main geometry and the slicing of the worm gear set as well as the various contact lines that take place along the tooth flank during meshing for a given instant of time. Note that the number of contact lines is determined by the magnitude of the contact ratio. Each slice on the worm and gear can then be modelled as a spur gear if the width of the slice is made relatively small. Therefore, the accuracy of results will depend on the number of the slices that represent both the worm and the gear. The more these slices, the better the results that are obtained. Moreover, spur gear slices on the worm will have the same root and outside diameters as the worm itself within the meshing zone, but their exact points of contact with their counterpart slices of the gear will depend on their location. On the other hand, the slices on the gear will have variable root and outside diameters depending on their location as shown in Figure (1). The face width of each slice of the set depends also on the geometry and the number of slices considered as shown in the figure.

Under this assumption, all theories suitable for 2D gears will be applicable. The procedure of this study does not only simplify the process of analysis, but more importantly, speeds up the computations.

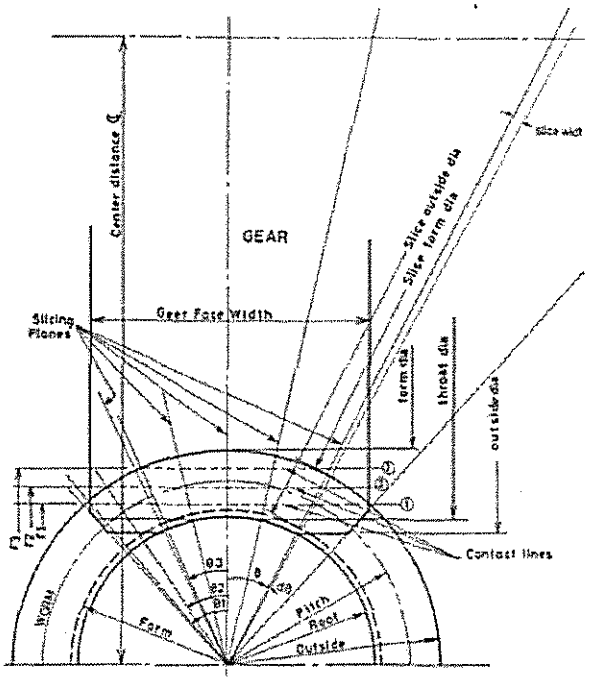

Fig. 1 : Contact lines & slicing planes

4. SLICE STIFFNESS AND DEFLECTION CALCULATION:

The primary objective of this analysis process is to obtain load distribution and stresses of engaging gears. Load distribution depends mainly upon tooth profile and elastic deformations of teeth and gear bodies. It is clear that at any instant of the engagement, the

total force being transmitted must balance the input force. But the load borne at an individual point of a tooth flank is determined by the mesh stiffness and the contact surfaces at the point, as there are a number of contact lines at any moment.

Theoretically, the mesh stiffness of a contact point between a pair of teeth is a function of the phase of mesh and the position along the tooth contact line.

Since both the worm and gear are represented by a series of spur gear slices, each slice on either the worm or gear is modeled as a straight spur gear whose main dimensions depend upon the location of the slice on the line of contact between meshing gears, and along the line of action of the slice. If a slice is subjected to a normal load F_{ij}, then the total deflection δ_{ij} is calculated from the equation given in [12] which accounts for bending, shear, foundation and compressive deformations. Referring to Figure (2):

$$\delta_{ij} = \delta_{B_{ij}} + \delta_{S_{ij}} + \delta_{G_{ij}} + \delta_{P_{ij}} \tag{8}$$

where

$\delta_{B_{ij}}$ = bending deflection

$$\frac{12\,F_{ij}\cos^2\phi\, z}{E\Delta b S_F^3}\left[S_m^2 + \frac{z^2}{3} - S_m z\right] + \frac{6F_{ij}\cos^2\phi(w-z)^3}{E\Delta b S_F^3} \left[\frac{(w-S_m)}{(w-z)}\left\{4 - \frac{(w-S_m)}{(w-z)}\right\} - 2\log_e\left[\frac{(w-S_m)}{(w-z)}\right] - 3\right] \tag{9}$$

$\delta_{S_{ij}}$ = deformation due to shearing

$$\delta_{S_{ij}} = \frac{2(1+\nu)F_{ij}\cos^2\phi}{E\Delta b S_F}\left[z + (w-z)\log_e\left(\frac{w-z}{w-S_m}\right)\right] \tag{10}$$

$$w = \frac{nS_F - zS_k}{S_F - S_k} \tag{11}$$

$\delta_{G_{ij}}$ = deformation due to the inclination of foundation under load

$$\delta_{G_{ij}} = \frac{24F_{ij}S_m^2\cos^2\phi}{\pi E\Delta b S_F^2} \tag{12}$$

$\delta_{P_{ij}}$ = compressive deformation

$$\delta_{P_{ij}} = \frac{4F_{ij}(1-\nu^2)}{\pi E\Delta b}\left(\frac{\rho_2}{\rho_1+\rho_2}\right) \tag{13}$$

where ρ_1 and ρ_2 are the radii of curvature at the contact point for the two meshing slice teeth. E is Young's modulus of elasticity and ν is Poisson's ratio. The rest of the symbols are explained in Figure (2).

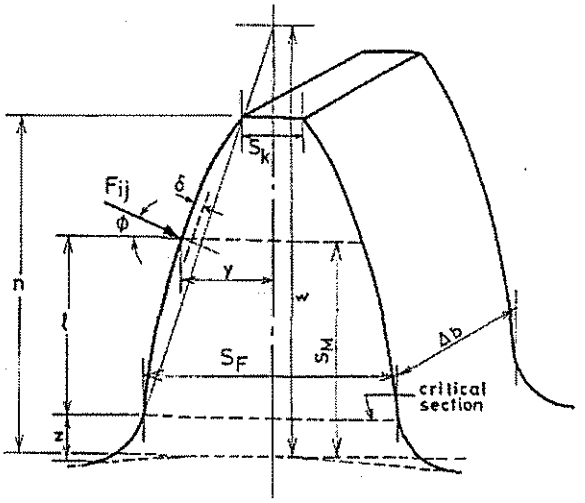

Fig. 2 : Tooth deflection and fillet stress parameters

The slice stiffness K_{ij} then becomes

$$K_{ij} = \frac{F_{ij}}{\delta_{ij}} \tag{14}$$

The stiffnesses of all slices on the worm and the corresponding ones on the gear can therefore be determined. It is clear that slice stiffness K_{ij} on a given line of contact depends upon the point of load application on the slice and the slice geometry.

The meshing teeth of both the worm and gear were modelled by a series of spur gear slices. Figure (3) shows a pinion slice and a gear slice in mesh. The face width of each slice depends on the number of slicing planes assigned to model the gear set. The more the number of planes, the lesser the face width of a slice and the greater the modeling accuracy of the actual gear set.

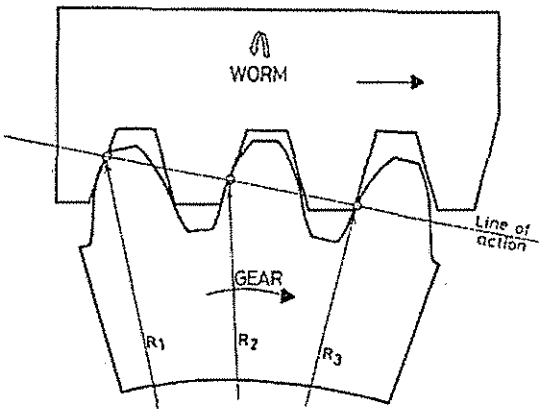

Fig. 3 : Line of action intersecting teeth of a slice

5. STIFFNESS CALCULATION AND LOAD DISTRIBUTION:

The line of action shown in Figure (3) intersects several adjacent teeth slices on the worm and gear, and the transmitted load is shared between those teeth segments. In order to determine the load sharing among these segments, a detailed stiffness analysis was carried out for all the segments on the worm and the corresponding ones on the gear. The worm and gear were sliced into a specified number of segments using the slicing planes shown in Figure (1). The teeth on each slice of either the worm or the gear were modeled as a series of springs whose stiffness was calculated using equations (8) to (14).

Due to the inherent flexibility of the meshing tooth slices, they deflect from their true position due to the applied load. Moreover, segments on the same line of contact of a given slice should experience equal deflections in order to maintain contact with mating teeth on corresponding slices and avoid physical overlap [12]. Therefore, the stiffness arrangement of the slices on the worm and the corresponding ones on the gear is shown schematically in Figure (4). The total normal transmitted load is distributed among the slices of the meshing teeth of the worm and gear. Each meshing slice on the worm will thus be subjected to a portion of the load depending upon its stiffness and the stiffness of the slice on the gear with which it is in mesh.

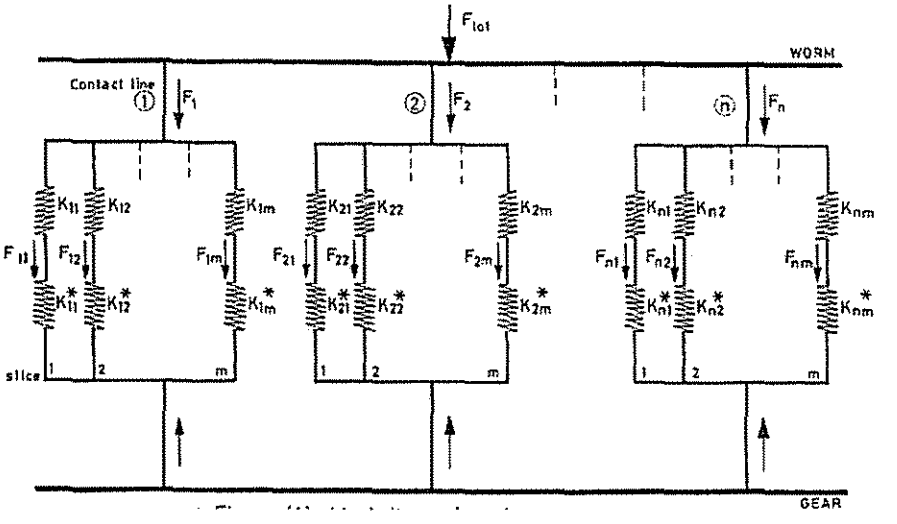

Fig. 4 : Modeling of entire gear set

In order to simplify the load sharing calculation, each slice on the worm, which is represented by a stiffness K_{ij}, is summed up with the stiffness of the corresponding slice on the gear K_{ij} *. The subscript i refers to the contact line order and the subscript j refers to the slice order on the line of contact. The number of slices on each line of contact was considered equal (m) for the sake of brevity. Since the two meshing stiffnesses on the worm and gear at each slice are connected in series, the equivalent stiffness $K_{eq_{ij}}$ is obtained from:

$$K_{eq_{ij}} = \frac{K_{ij}\, K^{*}_{ij}}{K_{ij} + K^{*}_{ij}} \qquad \begin{matrix} i = 1, 2, \ldots\ldots n \\ j = 1, 2, \ldots\ldots m \end{matrix} \tag{15}$$

where n is the total number of contact lines and m is the total number of slices on the contact lines. The stiffnesses that represent the equivalent ones of the meshing slices on the worm and gear on the same contact line i are then treated as a set of springs connected in parallel, since they experience the same deflection.

$$K_i = \sum_{j=1}^{m} K_{eq_{ij}} \qquad i = 1, 2, \ldots\ldots n \tag{16}$$

Similarly, the combined effect of all the stiffnesses of all the lines of contact can then be obtained from:

$$K_{tot} = \sum_{i=1}^{n} K_i \tag{17}$$

The individual tooth slice loading F_{ij} is therefore determined from the total transmitted load F_{tot} and slice stiffness K_{ij}, from the following two equations:

$$\frac{F_{ij}}{K_{eq_{ij}}} = \text{constant} \qquad \begin{matrix} i = 1, 2, 3, \ldots\ldots n \\ j = 1, 2, 3, \ldots\ldots m \end{matrix} \tag{18}$$

$$F_{tot} = \sum_{j=1}^{m} \sum_{i=1}^{n} F_{ij} \tag{19}$$

Equations (18) and (19) were solved to determine the individual loads F_{ij} as:

$$F_{ij} = \frac{K_{eq_{ij}}}{\sum_{k=1}^{n} \sum_{\ell=1}^{m} K_{eq_{k\ell}}} F_{tot} \tag{20}$$

Once the loads transmitted by the slices and the geometry of each slice are known, the gear set fillet stresses can be easily determined as discussed in the following section. It should be noted that, in case of overloading, the teeth may deform plastically and the linear relationship between slice load and deflection may become inapplicable. However, the procedure of the present study can still be used to determine areas prone to failure; i.e. pitting and spalling by calculating the magnitudes and locations of stresses resulted from applied loads.

6. TOOTH FILLET STRESS:

The distribution of tooth fillet tensile and compressive stresses σ_{ft} and σ_{fc} due to load distribution along contact lines was determined by calculating these stresses for all slices of the worm and gear. Aida and Terauchi formula for fillet stress calculation which is given in reference [12] for spur gears was applied to each slice as follows:

$$\sigma_{ft} = \left(1+0.08\frac{S_F}{z}\right)\left[0.66\sigma_b + 0.4\sqrt{\sigma_b^2+36\tau^2} + 1.15\sigma_c\right]\frac{F_{ij}}{\Delta b} \tag{21}$$

$$\sigma_{fc} = \left(1+0.08\frac{S_F}{z}\right)\left[-0.66\sigma_b - 0.4\sqrt{\sigma_b^2+36\tau^2} - 1.4\frac{\sin\phi}{S_F} + \frac{6y\sin\theta}{S_F^2}\right]\frac{F_{ij}}{\Delta b} \tag{22}$$

where:

$$\sigma_b = \frac{6\ell\cos\phi}{S_F^2}$$

$$\tau = \frac{\cos\phi}{S_F}$$

$$\sigma_c = \left(1+\frac{6y}{S_F}\right)\frac{\sin\phi}{S_F}$$

and the rest of the symbols are given in Figure (2).

Equations (21) and (22) do not account for any sliding action in the evaluation of stress. Nevertheless, they have been proven to be applicable in cases where surface fatigue failure takes place.

7. ANALYTICAL RESULTS AND DISCUSSIONS:

The forementioned procedure can be applied to investigate the mesh stiffness variation along tooth flank, the distribution of loads along lines of contact, and fillet stresses for, practically, any worm gear set under given running conditions. To gain recognition, the procedure was later applied to the gears given in [1], that were analyzed analytically using a Matrix transformation and a numerical procedure and experimentally using Laser Holographic Interferometry. Both gears given in [1] and in this study were running under same loading conditions. Fillet stress results obtained from [1] were then compared with those obtained when the procedure presented in this study is used. The main dimensions of the worm and gear used in all methods of analysis are given in table (1). The applied worm torque was equal to 9.8 N.m. First, the stiffness, load and stress results obtained from the present study, will be presented and later on, the stress results obtained from this study will be compared with those obtained from [1].

Table 1: Gear Specifications

		Worm	Gear
Module	(mm)	6.2	
Pressure angle	(deg)	20	
Lead angle	(deg)	17.896	
Center distance	(mm)	125	
Number of teeth		3	31
Pitch circle diameter	(mm)	57.6	192.4
Averaged diameter	(mm)	57.8	192.2
Outside diameter	(mm)	68.0	204.8
Root diameter	(mm)	41.2	178.0
Face width	(mm)	--	46

7.1 Stiffness Distribution:

The stiffness of all the spur gear slices, that represent the actual worm gear set, were calculated for both the worm and gear using equations (8) to (14). A total of 20 slices has been used in this study. However, the accuracy of the results did not improve significantly by using more slices. For an instant of time when an end tooth slice on the worm is about to begin meshing was chosen for analysis. It was found that there exist three lines of contact at this given instant of time. The radii, measured on the worm, for the three lines of contact were designated r_1, r_2 and r_3 as shown in Figure (1) and were found to be 27.32, 28.80 and 31.42 mm, respectively. The contact lines embraced angles designated by θ_1, θ_2 and θ_3 and they were found to be 36.53, 32.11 and 22.46 degrees, respectively, as shown in the same figure. The stiffness variation along the three lines of contact was plotted against angle θ, defined in Figure (1), and the results are shown in Figure (5). It is clear, from the figure, that the gear stiffness is several times the worm stiffness. This is mainly due to the proximity of the three contact lines to the tip of the worm (and consequently to the root of the gear) for the instant of mesh under consideration and the tooth deflection in general, is higher at the tip than at the root. For the same argument it was found that the tooth stiffness of the gear reaches minimum at the throat area of the gear, whereas it is maximum for the worm. The equivalent stiffness, calculated from equation (15), was found to be almost uniform along the three lines of contact with a small increase at the throat section.

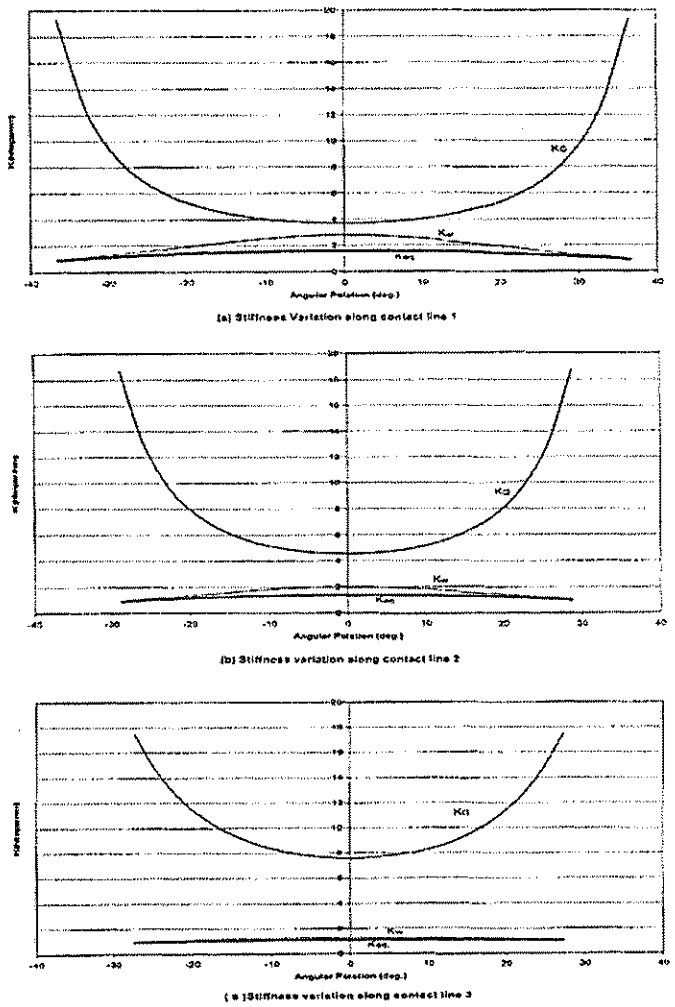

Fig. 5 : Stiffness variation on contact lines

7.2 Load Distribution Along Lines Of Contact:

The transmitted (contact) loads along the lines of contact were calculated from equation (20) for all the slices that represent both the worm and gear. The load results are presented graphically in Figure (6) against the worm angular position of θ. The figure indicates that the transmitted loads reach their maximum values close to the throat area of the gear for the three lines of contact. The load distribution varies for each individual line of contact with a maximum variation of 72% for line 1 and minimum variation of 20% for line 3. It is also clear that the load distribution along the lines of contact follows the same trend of the equivalent stiffness distribution presented in Figure (5) which is a common practice in gear design. So, one can state that transmitted loads in meshing gears change according to change in equivalent stiffness of the engaged teeth.

7.3 Tooth Fillet Stress Distribution:

The procedure outlined in this study is capable of calculating both the tensile and compressive stress as given by equations (21) and (22). However, it was decided to

investigate the effect of the tensile stress only; since it is the dominant cause of tooth fillet failure. Therefore, tensile tooth fillet stress distribution for all the slices that resemble the worm and gear under the outlined loads shown in Figure (6) are carried. The tensile stress distribution of the worm due to applied loads on all contact lines are shown in Figure (7) which indicates that the stress distribution follows the same trend, to a certain extent, as the load distribution, i.e. it peaks at the throat section of the gear and tends to decay close to the ends of the contact lines for the first and second contact lines. As for the third contact line, the stress variation seems to be relatively uniform, mainly because the length of the third contact line is shorter than the other two lines and it is located close to the tip of the worm where the bending moment arm is maximum. It should also be pointed out that the magnitude of the fillet stress depends on two main factors as shown in equation (21): the applied load F_{ij} and the moment arm ℓ. The maximum value and location of the fillet stress vary as these two factors, together, vary.

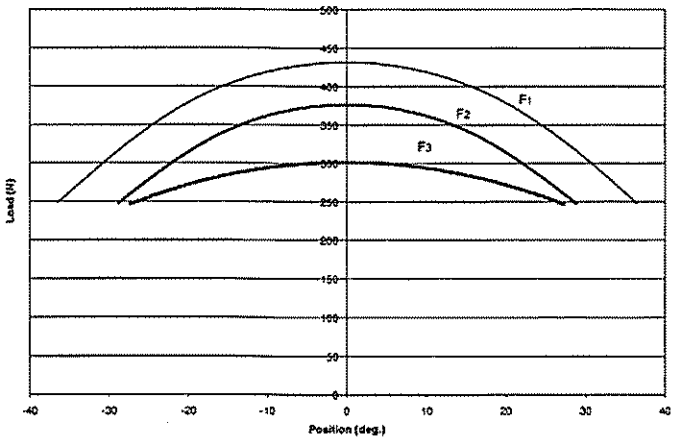

Fig. 6 : Load distribution on contact lines

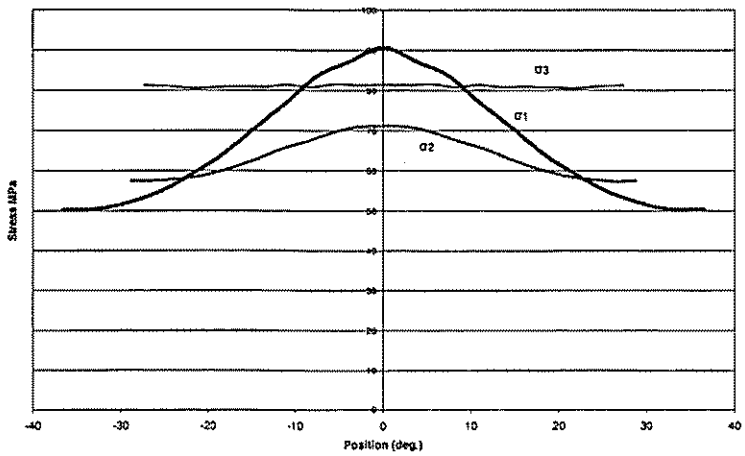

Fig. 7 : Worm Tensile Fillet Stress vs. Angular Position for all contact lines

8. SUBSTANTIATION OF ANALYTICAL RESULTS:

The analytical results obtained by the procedure outlined in this study and using the gears described in table 1 are verified by the results given in [1] using both matrix transformation and Laser Holographic Interferometry. In the present study, the tensile fillet stress for each slice was calculated from equation (21) using the applied load per slice and the slice geometry. The results were superimposed on those obtained in [1] as shown in Figure (8) which indicates that the stresses calculated by the procedure outlined in this study are in the same order of magnitude as those obtained in [1] and therefore, agree reasonably well with them. Interestingly, the experimental results are in close agreement with those presented in this study.

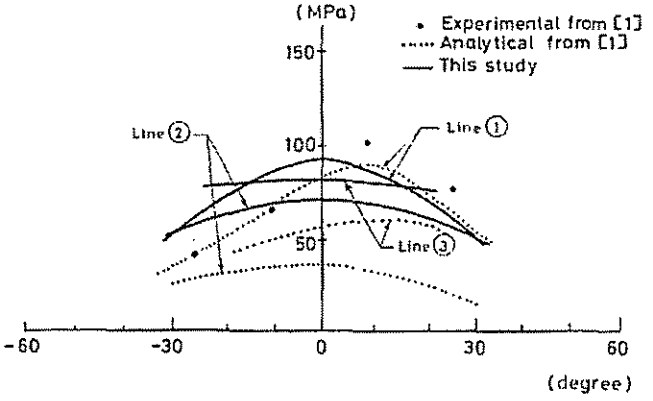

Fig. 8 : Worm Fillet Stress
(comparison of results)

9. CONCLUSION:

An analytical procedure for calculating tooth loading and stresses in straight worm gearing is presented. The procedure is based upon the assumption that a worm gear set can be modelled as a set of spur gear slices having predetermined geometries and that the slice stiffness of both gears are dependent on tooth geometry and point of load application. The analytical results obtained correlate well with those obtained from literature using matrix transformation and laser optical interferometry.

The model predicts individual tooth load distribution along lines of contact between the worm and the gear. It also gives tooth stiffness variation along the meshing tooth flank.

From the tooth loading and gear geometry, fillet stresses of both worm and gear can readily be determined. The forementioned conclusions confirm that the analytical procedure presented in this study is reliable and useful since it predicts acceptable results in a very short time as compared to the time required for using other analytical or numerical methods.

The developed technique can be programmed using any computer language such as BASIC, FORTRAN, MATLAB, C., ...etc. and the results are obtainable almost instantly.

10. ACKNOWLEDGMENT:

The authors wish to acknowledge the sponsorship provided by the Research Administration of Kuwait University in supporting research.

11. REFERENCES:

1] Sudoh, K., Tanaka, Y., Matsumoto, S., and Tozaki, Y., "Load Distribution Analysis Method for Cylindrical Worm Gear Teeth", JSME, Series C, Vol. 39, No. 3, pp. 606-613, 1996.

2] Zhang, J.J., Esat, I.I., and Shi, Y.H., "Load Analysis with Varying Mesh Stiffness", Computers and Structures 70, pp. 273-280, 1999.

3] Greening, J.H., Barlow, R.J., and Loveless, W.G., "Load Sharing on the Teeth of Double Enveloping Worm Gear", ASME Int. Power Trans. And Gearing Conf., San Francisco, Calif., pp. 1-6, August 1980.

4] Shimachi, S., Gunbara, H., Kobayashi, T., and Kawada, H., "Hourglass Worm Gears Designed to Concentrate Surface Normals", JSME Series C, Vol. 37, No. 2, pp. 347-354, 1994.

5] Su, D., Yang, F., Gentle, C.R., "A New Approach Combining Numerical Analysis and Three Dimensional Simulation for Design of Worm Gearing with Preferable Localized Tooth Contact", ASME Design Engineering Technical Conference, Atlanta, GA, September 1998.

6] Yang, F., Su, D., and Gentle, C.R., "Finite Element Modelling and Load Share Analysis for Involute Worm Gears with Localized Tooth Contact", Proc. Instn. Mech. Engrs., Vol. 215, Part C, pp. 805-816, 2001.

7] Simon, V., "Stress Analysis in Double Enveloping Worm Gears by Finite Element Method", ASME Journal of Mechanical Design, Vol. 115, pp. 179-185, March 1993.

8] Datong, Q., and Dongxing, Q., "Load Sharing and Contact of Hourglass Worm Gearing", Chinese Journal of Mechanical Engineering, Vol. 12, No. 4, pp. 260-265, 1999.

9] Bair, B.W., and Tsay, C.B., "ZK-Type Dual-Lead Worm and Worm Gear Drives: Contact Teeth, Contact Ratios and Kinematic Errors", ASME Journal of Mechanical Design, Vol. 120, pp. 422-428, Sept. 1998.

10] Buckingham, E., and Ryffel, H.H., "Design of Worm and Spiral Gears", Industrial Press Inc., 1981.

11] Shigley, J.E., "Mechanical Engineering Design", 1st Metric Ed., McGraw-Hill, New York, pp. 552-557, 1987.

12] Elkholy, A.H., "Tooth Load Sharing in High-Contact Ratio Spur Gears", ASME Journal of Mechanisms, Transmissions, and Automation in Design, Vol. 107, pp. 11-16, 1985.

NOMENCLATURE:

C	=	center distance
CR	=	contact ratio
E	=	Modulus of elasticity
F_{ij}, F_{tot}	=	force per slice and resultant of applied forces, respectively
K_{ij}, K^*_{ij}	=	slice stiffness of worm and gear, respectively
$K_{ij_{eq}}$	=	equivalent stiffness
L	=	lead
ℓ, S_M, S_F, S_K, z, w, n, Δb, y, r	=	dimensions given in Figure (2)
N	=	number of teeth/starts
p_t	=	circular pitch
p_x	=	axial pitch
R	=	pitch radius
R_b	=	base radius
R_f	=	form radius
R_o	=	outside radius
R_r	=	root radius
α,β	=	characteristic parameters
δij	=	tooth total deflection
$\delta_{B_{ij}}$, $\delta_{G_{ij}}$, $\delta_{P_{ij}}$, $\delta_{S_{ij}}$	=	bending, foundation, compressive and shear deflections, respectively
Δb	=	slice face width
ϕ	=	pressure angle
λ	=	lead angle
ν	=	Poisson's ratio
ρ	=	radius of curvature
σ_{ft}, σ_{fc}	=	tensile and compressive fillet stresses, respectively
ψ	=	helix angle

Subscripts

1, 2	=	refer to worm and gear, respectively